Article

Study on Health Indicator Construction and Health Status Evaluation of Hydraulic Pumps Based on LSTM–VAE

Zhenbao Li [1,2], Wanlu Jiang [1,2,*], Xiang Wu [1,2], Shuqing Zhang [3] and Dongning Chen [1,2]

1   Hebei Province Key Laboratory of Heavy Machinery Fluid Power Transmission and Control, Yanshan University, Qinhuangdao 066004, China
2   Key Laboratory of Advanced Forging & Stamping Technology and Science Ministry of Education of China, Yanshan University, Qinhuangdao 066004, China
3   School of Electrical Engineering, Yanshan University, Qinhuangdao 066004, China
*   Correspondence: wljiang@ysu.edu.cn

Abstract: This paper addresses the difficulty of evaluating operating status in widely used gear pumps. A method for constructing hydraulic pump health indicators and evaluating health status is proposed based on LSTM–VAE. In this study, the vibration signal data source of gear pumps was assessed in the accelerated life test. Firstly, the normalized feature vectors of the whole-life operation data of gear pumps were extracted by wavelet packet decomposition and amplitude feature extraction. Combining an LSTM algorithm with a VAE algorithm, a method for constructing hydraulic pump health indicators based on LSTM–VAE is proposed. By learning the feature vectors of gear pumps in varying health conditions, a one-dimensional HI curve of the gear pumps was obtained. Then, LSTM was used to predict the HI curve of gear pumps. According to the volume efficiency of the gear pumps, the health status of gear pumps is divided into four states: health, sub-health, deterioration, and failure. The health status of the hydraulic pump is accurately evaluated by the health indicator. Finally, the proposed method is compared with the traditional method based on feature selection and PCA dimensionality reduction. The health indicator constructed by the method proposed in this paper is superior to the traditional method in terms of tendency, robustness, and monotonicity, which proves the effectiveness of the method proposed in this paper.

Keywords: gear pump; long short-term memory neural network; variational auto-encoder; indirect health indicator; health assessment

1. Introduction

With the progress of science and technology, the level of intelligence and integration of mechanical equipment has been continuously improved. At the same time, the internal structure has become increasingly sophisticated [1]. The failure of one component affects the normal operation of the entire piece of equipment. Hydraulic servo systems have high power density, high precision, and fast response and have been widely used in engineering machinery, metallurgical machinery, mining machinery, aerospace, and other fields [2]. As the "heart" of the hydraulic system, the hydraulic pump converts the mechanical energy of the prime mover into the pressure energy of the hydraulic system and continuously supplies the hydraulic cylinder, hydraulic motor, and other actuators [3]. The health condition of the hydraulic pump directly determines the operation of the whole hydraulic system. Once the hydraulic pump fails, it affects the normal operation of the equipment and can cause significant economic losses and even casualties [4,5]. Therefore, it is particularly important to evaluate the health status of a hydraulic pump and guide its condition-based maintenance (CBM) [6,7].

The essence of a health status assessment is to model the performance failure degradation process of equipment and evaluate its current health status and subsystems by

using current monitoring data and historical data [8,9]. In essence, health status assessment models the degradation state of the system and then constructs a one-dimensional health indicator (HI) curve of the system to characterize the performance degradation or deviation degree from the normal state [10]. HI curves can be divided into the direct HI and indirect HI according to different calculation methods. The direct HI is based on the primary data, according to expert empirical knowledge, and directly constructs a health value with physical significance through simple feature extraction [11], for example, the root mean square (RMS) of a mechanical equipment vibration signal [12,13], power spectral density [14], and mathematical model spectrum [15]. The indirect HI is usually obtained by fusing time-domain features or frequency-domain features of the primary data with machine learning and other methods. It has no real physical meaning and is also known as the virtual HI, and methods such as principal component analysis technology are used to extract the HI value [16], along with self-organizing mapping technology to construct the HI value of equipment [17] and fusion multi-sensor data in the assessment of equipment health status [18].

Although the modeling method of health assessment has achieved strong theoretical results, in the practical application process, due to the complexity and diversity of the field equipment, a modeling method only relying on manual participation is difficult to widely use [19]. Due to the complex working conditions and harsh working environment of most hydraulic equipment, the difficulty of modeling increases exponentially [20,21]. Therefore, reducing manual intervention, automatically extracting effective information from signals, and ensuring universality are the development trends in equipment health assessment methods.

With the development of algorithm theory and the accumulation of massive data, deep learning technology shows incomparable advantages over traditional machine learning technology and has achieved excellent results in many fields [22,23]. However, deep learning is still in the exploratory research stage in the field of device health assessment. Tamilselvan et al. reported an aero-engine health state classification model based on deep belief networks (DBNs) [24]. Zhao Guangquan et al. developed a rolling bearing health status assessment method based on a stacked auto encoder (SDAE) [25]. Although deep learning technology has achieved some research results in the field of health assessment, there are few studies on health assessment methods for hydraulic systems with complex models and a harsh working environment.

To address the difficulty of extracting vibration signal characteristics and evaluating the operating status of hydraulic pumps [26], a method for constructing hydraulic pump health indicators and health status evaluation based on long short-term memory (LSTM) and a variational auto-encoder (VAE) is proposed. Firstly, the characteristics of the gear pump were obtained with wavelet packet decomposition and amplitude feature extraction. Then, a method for constructing a hydraulic pump health indicator based on LSTM–VAE was developed, and a one-dimensional HI curve of the gear pump was obtained. The constructed health indicators were used to evaluate the running state of gear pumps. Finally, the proposed gear pump health indicator construction method was compared with the traditional method for monotonicity, robustness, and trendability, and the experimental results showed that the proposed method is effective and advanced.

2. Feature Extraction and Feature Selection

2.1. Wavelet Packet Energy Feature Extraction

The wavelet packet transform analysis method is a technical improvement of the wavelet transform analysis method. It is a joint signal analysis method based on time and frequency domains. The method of wavelet packet decomposition can perform orthogonal decomposition of the collected signals in all frequency bands. An orthonormal basis that can reflect the original characteristics of the signals can be obtained by reasonably selecting the optimal wavelet packet basis function and the decomposition layer number.

Compared with wavelet transform, wavelet packet transform improves the ability of local refinement in the frequency domain of the signal, and the application of wavelet packet decomposition can achieve a more comprehensive frequency-domain analysis of the signal. The vibration signal is decomposed by the wavelet packet, and the energy characteristics of each frequency band are extracted as the characteristics of the signal.

The original signal is decomposed by a three-layer wavelet packet, and the decomposition tree structure is shown in Figure 1. The signal $x(i)$ is decomposed by the wavelet packet. The signal energy at the k-th node of the wavelet packet is calculated by the following formula:

$$E_k = \sum_{i=1}^{N} x_k(i)^2, \tag{1}$$

where $x(i)$ is the reconstructed signal at the k-th node of the wavelet packet, and N is the length of the sample signal.
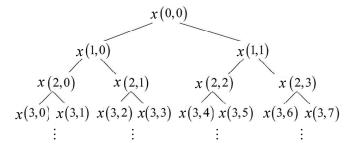

Figure 1. The structure of a wavelet packet decomposition tree.

We define $F = [F_1, F_2, \ldots, F_{34}]$ as the eigenvector, and the first 16 features are three-layer wavelet packet energy decomposition features, namely:

$$F_i = E_i, \ i = 1 \sim 16 \tag{2}$$

2.2. Time–Frequency Domain Feature Extraction

Usually, the dimensionless indicators are not directly affected by the operation of the mechanical equipment and are only determined by its corresponding probability density function; the dimensional indicators are directly affected by the operation of the mechanical equipment. Both dimensionless and dimensionless indicators can directly or indirectly reflect the evolution trend of performance degradation during gear pump operation [27]. The calculation method of the time-domain characteristic parameters of the vibration signals is shown in Table 1, where $x(i)$ is the vibration signal, $i = 1, 2, 3, \ldots, N$.

Table 1. Time-domain feature extraction method.

Time-Domain Feature	Calculation Method	Feature Representation
Mean value	$\overline{X} = \frac{1}{N} \sum\limits_{i=1}^{N} x(i)$	F_{17}
Variance	$\sigma^2 = \frac{1}{N-1} \sum\limits_{i=1}^{N} [x(i) - \overline{X}]^2$	F_{18}
Root mean square value	$X_{\text{rms}} = \sqrt{\frac{1}{N} \sum\limits_{i=1}^{N} x(i)^2}$	F_{19}
Kurtosis	$K = \frac{1}{N} \sum\limits_{i=1}^{N} x(i)^4$	F_{20}
Peak value	$X_{\max} = \max[|x(i)|]$	F_{21}
Root amplitude	$X_{\text{r}} = \left[\frac{1}{N} \sum\limits_{i=1}^{N} \sqrt{|x(i)|} \right]^2$	F_{22}
Peak-to-peak value	$X_{\text{pp}} = \max[x(i)] - \min[x(i)]$	F_{23}

Table 1. *Cont.*

Time-Domain Feature	Calculation Method	Feature Representation
Absolute mean value	$\|\overline{X}\| = \frac{1}{N}\sum\limits_{i=1}^{N}\|x(i)\|$	F_{24}
Standard deviation	$\sigma = \sqrt{\frac{1}{N}\sum\limits_{i=1}^{N}\left[x(i)-\overline{X}\right]^2}$	F_{25}
Shape factor	$S_f = \frac{X_{rms}}{\|\overline{X}\|}$	F_{26}
Crest factor	$C_f = \frac{X_{max}}{X_{rms}}$	F_{27}
Impulse factor	$I_f = \frac{X_{max}}{\|\overline{X}\|}$	F_{28}
Kurtosis index	$K_v = \frac{K}{X_{rms}^4}$	F_{29}
Clearance factor	$CL_f = \frac{X_{max}}{X_r}$	F_{30}

The feature extraction method based on the time domain is often unable to accurately judge the performance degradation trend of the mechanical equipment. Therefore, the feature extraction method based on frequency-domain characteristics is proposed. Firstly, the acquisition time domain signals are processed by fast Fourier transform (FFT), and the time-domain characteristics of these vibration signals are transformed into the frequency domain. The correlation of the frequency-domain characteristic parameters is shown in Table 2:

Table 2. Frequency-domain feature extraction method.

Frequency-Domain Feature	Calculation Method	Feature Representation
Gravity frequency	$CF = \dfrac{\sum\limits_{k=0}^{k_{max}}[f \times S(k)]}{\sum\limits_{k=0}^{k_{max}} S(k)}$	F_{31}
Mean square frequency	$MSF = \dfrac{\sum\limits_{k=0}^{k_{max}}[k^2 \times S(k)]}{\sum\limits_{k=0}^{k_{max}} S(k)}$	F_{32}
Frequency variance	$FV = MSF - (CF)^2$	F_{33}
Average power	$f_1 = \dfrac{\sum\limits_{k=0}^{k_{max}} S(k)}{k_{max}}$	F_{34}

In the formula, f_{max} is the upper bound of the analysis frequency band, and $S(f)$ is the amplitude of the power spectrum at frequency f.

2.3. Health Indicator Evaluation Index

(1) Monotonicity

In the actual production process, the actual health indicator curve of the equipment should be increased or decreased monotonically. References [28–30] provide the calculation method of monotonicity. When the health curve of a device is **H**, its monotonicity can be expressed as:

$$Mon(\boldsymbol{H}) = \frac{1}{K-1}\left| No.of\frac{d}{dh} > 0 - No.of\frac{d}{dh} < 0 \right| \tag{3}$$

Here, $\boldsymbol{H} = \{h_k\}_{k=1:K}$ is the health indicator value sequence of the system; h_k represents the health indicator value of the device at time t_k, and K represents the length of the health indicator value curve of the device system; $\frac{d}{dh} = h_{k+1} - h_k$ represents the differential of adjacent health indicator values in the sequence; and $No.of\frac{d}{dh} > 0$ and $No.of\frac{d}{dh} < 0$ represent the count value with positive difference and negative difference, respectively. The value range of $Mon(\boldsymbol{H})$ is between 0 and 1. Usually, the larger the value, the better the monotonicity.

(2) Robustness

Since the acquisition data are susceptible to external and self-generated noise interference in the process of data acquisition, the stability of the prediction results is seriously affected. Therefore, a suitable health state assessment algorithm is robust against external disturbances, and the health indicator value curve should smoothly show the equipment failure and degradation. The calculation method of the robustness is proposed in reference [29]:

$$Rob(\boldsymbol{H}) = \frac{1}{K}\sum_{k=1}^{K} \exp\left(-\left|\frac{h_k - h_k^S}{h_k}\right|\right) \tag{4}$$

Here, h_k^S represents the average trend value of the health indicator value at time t_k. The value of $Rob(\boldsymbol{H})$ ranges from 0 to 1, and the larger the value, the better the robustness.

(3) Trendability

Normally, the health indicator value curve of the equipment is related to the features and operation time of the equipment, which is defined as the trendability in reference [31]. The trendability index is employed to evaluate the fitness of every feature. A higher absolute value of this index means that the feature has a better tendency, which is helpful for condition monitoring and RUL prediction, and the specific calculation method is:

$$Tre(\boldsymbol{H}, \boldsymbol{T}) = \frac{\left| K\left(\sum_{k=1}^{K} h_k t_k\right) - \left(\sum_{k=1}^{K} h_k\right)\left(\sum_{k=1}^{K} t_k\right) \right|}{\sqrt{\left[K\sum_{k=1}^{K} h_k^2 - \left(\sum_{k=1}^{K} h_k\right)^2\right]\left[K\sum_{k=1}^{K} t_k^2 - \left(\sum_{k=1}^{K} t_k\right)^2\right]}}, \tag{5}$$

where t_k is the k-th moment in the sensor timing data, and h_k is the health indicator value at t_k. The value range of $Tre(\boldsymbol{H}, \boldsymbol{T})$ is 0~1. When it is close to 1, the health value has a strong correlation with the running time.

3. Variational Auto-Encoder (VAE) and LSTM Neural Network

3.1. Variational Auto-Encoder (VAE)

By constructing a neural network structure with a small number of hidden layers, the auto-encoder can obtain the encoding vector by nonlinearly mapping the input vector to the intermediate hidden layer, and then the decoder can reconstruct the input vector with as little error as possible. As an unsupervised deep learning algorithm, the most important role of an auto-encoder is to learn the salient features in the original data through hidden layers of smaller dimensions.

A variational auto-encoder (VAE) is a kind of deep generative model. Firstly, the variational probability distribution of variables is generated by variational reasoning on the original data, which is the encoder encoding process. Then, the training data are reconstructed according to the probability distribution of the generated variables, which is the decoding process. The VAE encoding and decoding process is shown in Figure 2.
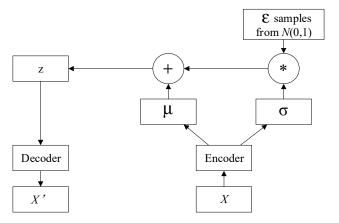

Figure 2. The encoding and decoding process of the VAE.

The VAE model consists of two parts; the encoder encodes the original data sample x into the intermediate hidden variable z, and the decoder decodes it into the original data space, which can be expressed as:

$$z \sim \mathrm{Enc}(x) = q(z|x), \tag{6}$$

$$\widetilde{x} \sim \mathrm{Dec}(z) = p(x|z). \tag{7}$$

VAE regularizes the encoder by applying a prior probability to the distribution of hidden variables and usually selects $z \sim N(0, I)$. The loss items of the VAE can be expressed as follows:

$$L_{\mathrm{VAE}} = -E_{q(z|x)}\left[\log \frac{p(x|z)p(z)}{q(z|x)}\right] = L_{\mathrm{llike}}^{\mathrm{pixel}} + L_{\mathrm{prior}}, \tag{8}$$

where

$$L_{\mathrm{llike}}^{\mathrm{pixel}} = -E_{q(z|x)}[\log p(x|z)], \tag{9}$$

$$L_{\mathrm{prior}} = D_{KL}(q(z|x)\|p(z)), \tag{10}$$

and where D_{KL} is the Kullback–Leibler divergence.

3.2. LSTM Neural Network

In deep learning, the input of each layer of the fully connected deep neural network (DNN) and the convolutional neural network (CNN) is only related to the previous layer. In sequential samples, such as language processing, speech recognition, and text translation, the order of sample appearance is very important. Therefore, with this requirement, the recurrent neural network (RNN) is derived, which inputs the output of the previous $(t-1)$ time steps and the input at time t into the next layer, so as to process the time series more effectively. Although the RNN has unique advantages in dealing with time series, it is similar to other deep learning models in that more hidden layers cause gradient disappearance or gradient explosion. Gradient explosion can be easily solved by using gradient pruning, but the long-term dependence problem is difficult to solve. Therefore, researchers have proposed a series of solutions, among which LSTM is a very effective sequential model.

The LSTM network module is shown in Figure 3, among which the most important component is the state unit, which is the internal cycle of LSTM units used to preserve long-term memory. The state unit of LSTM is similar to a chain connected together, and information can flow along the connected state unit. LSTM uses forget gates, input gates, and output gates to remove or add information in the state unit.
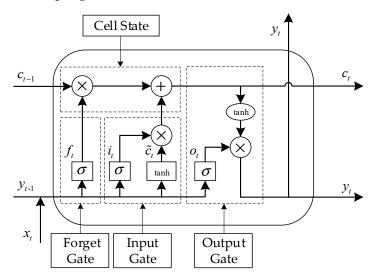

Figure 3. The LSTM network module.

In the LSTM prediction model, the first step is to determine the information to be retained in the state unit according to the output value of the forget gate. x_t and y_t are defined as the input and output of the state unit; then, the output value of the forget gate f_t is:

$$f_t = \sigma(W_f \cdot [y_{t-1}, x_t] + b_f), \tag{11}$$

where σ is the sigmoid function, y_{t-1} is the output value of the last state unit in the sequence, x_t is the input of the state unit at time t, and W_f and b_f represent the weight and bias of the forget gate, respectively.

The second step determines which input information is stored in the state unit. This step includes two parts. The first part is an input gate layer that determines which values are used to update through the sigmoid function, and the second part is a tanh layer that generates new candidate values $\widetilde{c}_t$ that may be added to the state unit. The specific calculation process is as follows:

$$i_t = \sigma(W_i \cdot [y_{t-1}, x_t] + b_i), \tag{12}$$

$$\widetilde{c}_t = \tanh(W_c \cdot [y_{t-1}, x_t] + b_c), \tag{13}$$

where W_i and b_i represent the weight and bias of the input gate, respectively, and W_c and b_c represent the weight and bias when the input gate creates a new candidate value, respectively. The method of updating the state c_{t-1} of the previous state unit to the state c_t of the current state unit is as follows:

$$c_t = f_t \cdot c_{t-1} + i_t \cdot \widetilde{c}_t. \tag{14}$$

Finally, LSTM generates an output based on the state of the state unit. Firstly, an initial output is obtained by the sigmoid function; then, the tanh function is used to scale the state value of the state unit to between -1 and 1, multiplied by the output obtained by the sigmoid function to obtain the final output of the state unit. The specific calculation process is as follows:

$$o_t = \sigma(W_o \cdot [y_{t-1}, x_t] + b_o), \tag{15}$$

$$y_t = o_t \cdot \tanh(c_t), \tag{16}$$

LSTM networks more easily learn long-term dependencies than ordinary RNN and have achieved great success in challenging sequence processing.

4. Health Assessment Model Based on LSTM–VAE

Aiming at the shortcomings of the existing time-domain sequence processing methods, such as over-dependence on expert experience and lack of generality in artificial feature extraction, this paper proposes a new data-driven device health assessment method by flexibly combining the LSTM network and VEA model.

After artificial feature information extraction of the mechanical equipment, the obtained multidimensional feature is the time series based on the equipment running time, and there is also a correlation between each feature [32]. The equipment health assessment method based on the LSTM network and VAE model proposed in this paper, on the one hand, can effectively extract time-series characteristics based on the LSTM network, and on the other hand, combined with the VAE method, the correlation between the original data and each dimension can be mapped to the hidden space to achieve deeper feature extraction. Moreover, combined with the VAE method, the continuous hidden space probability distribution model is robust to noise caused by sensors, equipment differences, and other factors.

4.1. Structure of LSTM–VAE Health Assessment Model

In order to extract the relationship between the vibration signal feature *F* and the time series, this study used the LSTM layer to replace the feedforward neural network

layer of the VAE. The expansion form of its internal structure along the time domain is shown in Figure 4. In the training stage of the LSTM–VAE model, the model was trained unsupervised by using the characteristics of the gear pump health status and adjusted of network parameters and learning features. After training, we input the characteristics of the gear pump's accelerated life data into the trained model to calculate the reconstruction error. The reconstruction error reflects the deviation between the current state and the health state of the gear pump. The health indicator of the gear pump at this time was obtained by processing the reconstruction error.
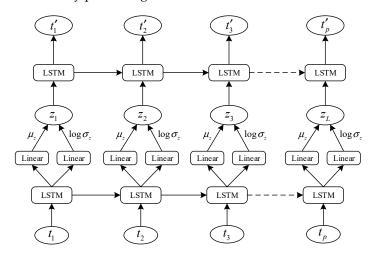

Figure 4. The expansion form of the LSTM–VAE encoder and decoder in the time domain.

4.2. Health Assessment Process of Gear Pump based on LSTM–VAE

The modeling method of the gear pump health assessment model based on the LSTM–VAE is shown in Figure 5, which includes the following steps:
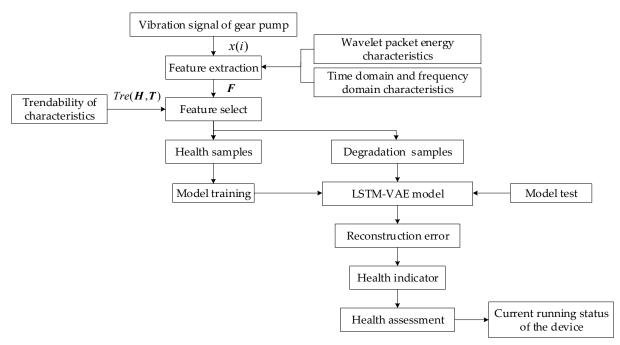

Figure 5. Health assessment process of gear pump.

(1) Obtaining the whole-life acceleration test data of the gear pump.

Through the step acceleration pressure test of the gear pump, the vibration signal $x(i)$ of the whole lifecycle of the gear pump and the flow signal $q(i)$ of the pump outlet

were obtained, where $i = 1, 2, \ldots, L$, and L is the maximum running time of the gear pump. During the test, acceleration sensors were installed in three directions (x, y, and z) of the end cover of each gear pump.

(2)   Feature extraction of data.

Wavelet packet energy features, time-domain features, and frequency-domain features were extracted from the vibration signal $x(i)$ of the whole lifecycle of the gear pump. Each feature was normalized to obtain the feature vector of the i-th feature $\boldsymbol{F}_{l,i} = [F_{1,i}, F_{2,i}, \ldots, F_{L,i}]$ in each running cycle, where L is the running time of the gear pump.

(3)   Feature selection.

The 34 features in the feature vector $\boldsymbol{F}$ were ranked according to the trendability parameters $Tre(\boldsymbol{H}, \boldsymbol{T})$ of a single feature, and the top 10 features with larger trendability parameters were selected to form the feature matrix $\boldsymbol{T}$.

(4)   LSTM–VAE model training.

The vibration data in the healthy state of the gear pump were used to train the model, and the sliding window was used to learn the distribution of gear pump characteristics in the healthy state. Assuming that the encoder input is $\boldsymbol{T} = \left[\boldsymbol{t}_1, \boldsymbol{t}_2, \ldots, \boldsymbol{t}_p\right]$, where p is the length of the time window, and the reconstructed output is $\boldsymbol{T}' = \left[\boldsymbol{t}'_1, \boldsymbol{t}'_2, \ldots, \boldsymbol{t}'_p\right]$, the reconstruction error at each time of the sample is as follows:

$$e_t = \left\| \boldsymbol{t}_t - \boldsymbol{t}'_t \right\|. \tag{17}$$

In the sliding process of the time window, multiple reconstruction errors were obtained at the same time point. Multiple reconstruction errors at the same time point were averaged to obtain the reconstruction error sequence $\boldsymbol{e}_t$ of the equipment, which was then normalized to obtain the health value curve of the equipment.

$$h_t = \frac{e_{\max} - e_t}{e_{\max} - e_{\min}}, \tag{18}$$

Here, $e_{\max}$ and $e_{\min}$ are the maximum and minimum reconstruction errors of the equipment, respectively; h_t is the health indicator of the gear pump at time t; and $0 \leq h_t \leq 1$.

(5)   The health status assessment of the gear pump.

The health status of the gear pump was divided according to the volumetric efficiency and health indicator of the gear pump. We obtained the health status of the type of gear pump division standard, and the standard was applied to the health status assessment of the gear pump.

5. Construction of the Gear Pump Health Indicator Based on LSTM–VAE
Composition of the Test System

The test system of this test was the gear pump full-life acceleration test bed, and a load was applied to the gear pumps during the test. The hydraulic system schematic diagram of the test bed is shown in Figure 6.

The vibration of the hydraulic pump includes not only the meshing vibration of the gear but also the mutual coupling of hydraulic shock vibration. The gear meshing vibration and hydraulic shock vibration are transmitted to the vibration sensor through the pump body. During the test, four gear pumps of the same model were operated at the same time, and acceleration sensors were installed in three directions (x, y, and z) of the end cover of each gear pump, as shown in Figure 7. The main component models and performance parameters used in the test bed are shown in Table 3.
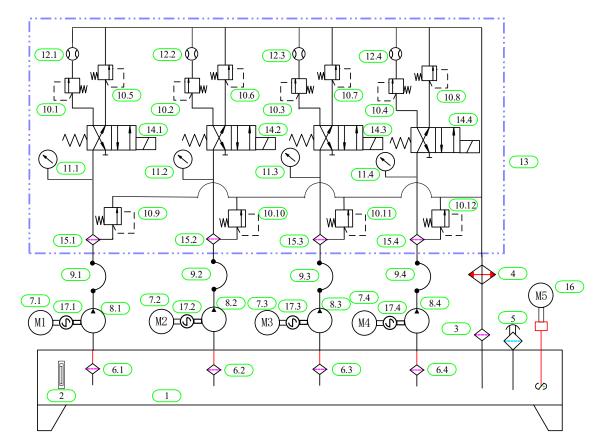
Figure 6. Hydraulic system schematic diagram of the gear pump accelerated-life test bed: **1**. Oil tank; **2**. Liquid level thermometer; **3**. Return oil filter; **4**. Air cooler; **5**. Air filter; **6**. Oil suction filter; **7**. Electric motor; **8**. Gear pump; **9**. High-pressure hose; **10**. Relief valve; **11**. Pressure gauge; **12**. Flow meter; **13**. Oil circuit block; **14**. Electromagnetic valve; **15**. High pressure filter; **16**. Blender; **17**. Torque speed meter.
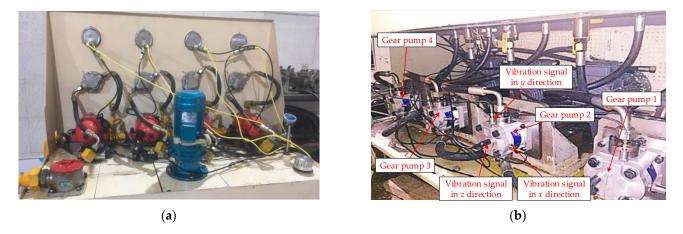

(**a**)

(**b**)

Figure 7. Lifecycle test bed of gear pump: (**a**) topside of test bed; and (**b**) underside of test bed.

In this study, the gear pump volumetric efficiency calculation method is:

$$\eta = \frac{q}{q_L} = \frac{q}{nQ_t},\tag{19}$$

where η is the volumetric efficiency of the gear pump, q is the actual flow, q_L is the theoretical flow, n is the motor speed, and Q_t is the theoretical discharge of the gear pump.

Table 3. The models and performance parameters of the main components of the test bed.

Serial Number	Component Name	Component Model	Performance Parameters of Component
1	Gear pump	CBWF-304	Preset pressure: 20 MPa, rated speed: 2500 r/min, nominal displacement: 4 mL/r
2	Flowmeter	MG015	Range of flow variation: 1~40 L/min
3	Acceleration sensor	YD-36D	Frequency range: 1 Hz~12 kHz
4	Pressure sensor	PU5400	Measuring range: 0~400 bar
5	Torque and rotational speed sensor	CYT-302	Torque range: 0~2 Nm, rotational speed range: 0–3000 r/min
6	Temperature sensor	CWDZ11	Measuring range: −50~100 °C
7	Data acquisition card	NI PXIe-6363	16-bit, 2 MS/s

There were four gear pumps designed in the whole-life test system of the gear pump. Each gear pump had a high pressure acceleration branch and rated working pressure branch. In the actual operation process of the gear pump, the pressure levels in high pressure branch were 21, 23, 25, and 27 MPa, and the pressure level in the rated pressure branch was 20 MPa. When gear pumps ran for 59 min 40 s on the high pressure accelerating branch, electromagnetic valve 14 started to work, gear pumps were transferred to the rated pressure branch for 20 s, and the vibration signal of gear pumps were collected in the last 2 s, as shown in Figure 8. The sampling frequency of the vibration signal was set to 12 kHz, and each of the four gear pumps ran for 1200 h.
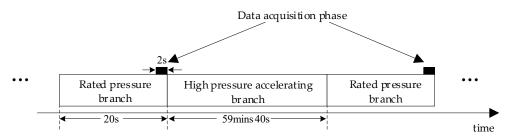

Figure 8. Vibration signal sampling settings.

In the whole-life test process of the gear pump, the oil temperature was set to 45–50 °C, and the four safety valves 10.9–10.12 were set to 30 MPa. In order to accelerate the performance degradation of the gear pump, the step pressure accelerated test method was adopted in the whole-life test bed. Compared with the constant pressure accelerated degradation test, it effectively reduced the test time and cost. At the same time, in the gear pump pressure loading, the pressure level used the pressure average deployment. The minimum acceleration pressure was set to 21 MPa, and the maximum acceleration pressure was set to 27 MPa. When the volumetric efficiency of the gear pump dropped by 10%, the pressure was raised to the next stage. When the volumetric efficiency of the four gear pumps was lower than 60%, all the gear pumps were considered as failed, and the test was stopped. The schematic diagram of the step pressure acceleration test is shown in Figure 9. According to the experimental results, $\tau_1 = 310$ h, $\tau_2 = 733$ h, $\tau_3 = 1028$ h and $\tau_4 = 1200$ h. At the end of the test, some parts of gear pump 1 were worn, as shown in Figure 10.

During the test, the data acquisition program written by LabVIEW was used to collect the gear pump vibration signal, pressure signal, flow signal, etc. We monitored the operation status of the gear pumps throughout their lifecycle.

According to the analysis, the vibration signal amplitude of the gear pump in the x and y direction was small, while the vibration signal amplitude in the z direction was large and had obvious regularity. Therefore, the vibration signals in the z direction of the gear pumps were selected as the analysis object in this study.

Firstly, the collected vibration signals were extracted and normalized; then, the trendability of the normalized features $Tre(\boldsymbol{X}, \boldsymbol{T})$ was calculated. The average values of the trendability parameters for each of the 34 characteristics of the four hydraulic pumps are

shown in Figure 11. The 34 features in the feature vector *F* were ranked according to the trendability parameters $Tre(H, T)$ of a single feature, and the top 10 features with the largest trendability parameters were selected to form the feature matrix *T*. The filtered feature codes and their trendability characteristics are shown in Table 4.
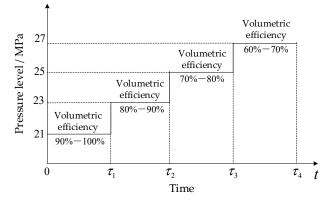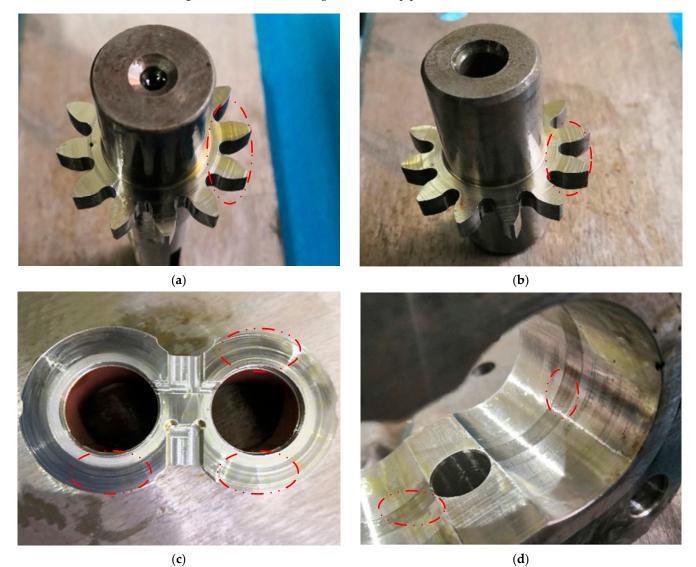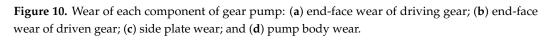

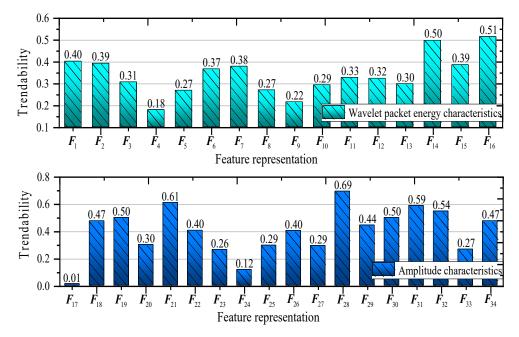**Figure 9.** The schematic diagram of the step pressure acceleration test.

(a)

(b)

(c)

(d)

Figure 10. Wear of each component of gear pump: (**a**) end-face wear of driving gear; (**b**) end-face wear of driven gear; (**c**) side plate wear; and (**d**) pump body wear.

Figure 11. The trendability parameters of each characteristic of gear pumps.

Table 4. The characteristics after selection and their trendability.

Feature Representation	Characteristics Interpretation	Trendability
F_{28}	Impulse factor	0.691164
F_{21}	Peak value	0.607977
F_{31}	Gravity frequency	0.585184
F_{16}	Wavelet packet energy characteristic E_{16}	0.544904
F_{14}	Wavelet packet energy characteristic E_{14}	0.514463
F_{32}	Mean square frequency	0.497961
F_{19}	Root mean square value	0.497791
F_{30}	Clearance factor	0.497791
F_{18}	Variance	0.473714
F_{34}	Average power	0.473714

Mechanical equipment has a rapid wear stage in the initial stage of operation, constant wear in the middle stage, and finally, a process of rapid performance degradation. Therefore, in this study, the vibration data of the first 5–30% of the normal state of the four gear pumps in the whole-operation lifecycle were selected as the training samples for the training of the model. The operational data during the lifetime of four gear pumps were used as test data to obtain the normalized health indicators of the four gear pumps according to Equation (18); the health indicator curve is shown in Figure 12.

As an effective feature dimension reduction method, the principal component analysis (PCA) method has been widely used in fault diagnosis and feature dimension reduction. The PCA method was used to reduce the dimensions of 34 dimensional features, and the first principal component after dimensionality reduction was normalized to obtain the health indicator based on the PCA method.

In order to describe the health indicators of the gear pumps quantitatively, the monotonicity, robustness, and trendability of the three indicators of the four gear pump health indicators were quantitatively described. In order to prove the effectiveness of the proposed method, the health indicators obtained in this study were compared with the main feature F_{28} and the health indicator based on the PCA method, as shown in Table 5. As can be seen from Table 5, compared with the main feature and the health indicator based on the PCA method, health indicator construction method proposed in this paper is superior in

terms of monotonicity, robustness, and trendability and can better reflect the performance degradation trend of the hydraulic pump.

Figure 12. Normalized health indicators of four gear pumps: (**a**) gear pump 1; (**b**) gear pump 2; (**c**) gear pump 3; and (**d**) gear pump 4.

Table 5. Comparative analysis of three evaluation indexes of health indicators.

Gear Pump	Evaluation Indexes	Feature F_{28}	Health Indicator Based on PCA Method	Health Indicators (Present Study)
Pump 1	Monotonicity	0.0083	0.0133	0.0259
	Robustness	0.8254	0.4796	0.9927
	Trendability	0.6426	0.2212	0.8909
Pump 2	Monotonicity	0.0242	0.0317	0.0442
	Robustness	0.8575	0.4856	0.9971
	Trendability	0.8093	0.1774	0.9525
Pump 3	Monotonicity	0.0217	0.0225	0.0117
	Robustness	0.8198	0.4887	0.9945
	Trendability	0.5231	0.1890	0.8272
Pump 4	Monotonicity	0.0167	0.0100	0.0375
	Robustness	0.8119	0.4847	0.9925
	Trendability	0.7882	0.2042	0.8703

Subsequently, the health indicator was used as the input for the LSTM model and predicted. During the operation of the pump, its known operation data were used to predict its health indicators at the next time step, and the prediction results are shown in Figure 13:

Then, the first 60% of the health indicator of the gear pumps was used as the training samples to predict the remaining 40% of the health indicator of the gear pumps. The prediction results and the prediction deviation are shown in Figure 14. The *Y*-axis in Figure 14 is the error value between the predicted health indicator and the actual health indicator.
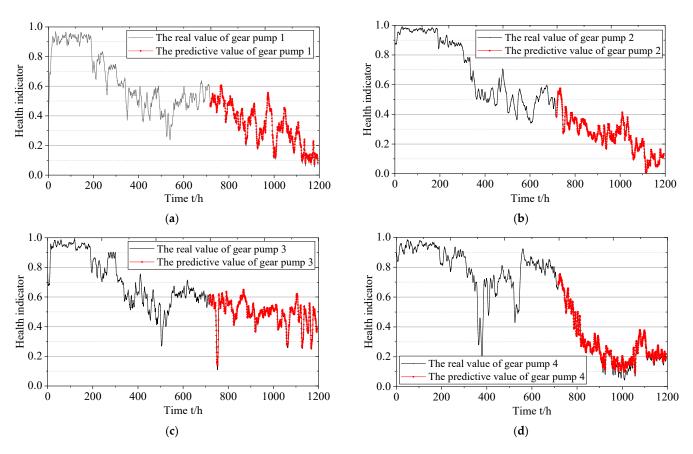
Figure 13. Health indicator prediction curve: (**a**) gear pump 1; (**b**) gear pump 2; (**c**) gear pump 3; and (**d**) gear pump 4.
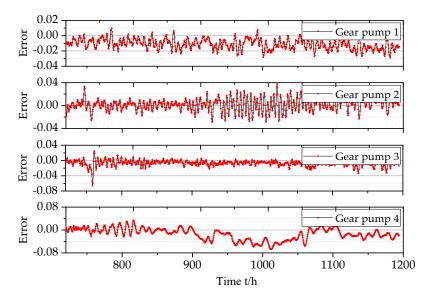

Figure 14. Prediction deviation curve.

Then, the same LSTM model was applied to predict the health value by using the health indicator, the most important feature F_{28}, and the first principal component after PCA dimension reduction as the features, and its error curve was drawn. The prediction error is the error between the predicted health indicator and the actual health indicator. The deviation box diagram of prediction error is shown in Figure 15. As can be seen from the figure, the prediction accuracy of the proposed method was high, and the error was small.
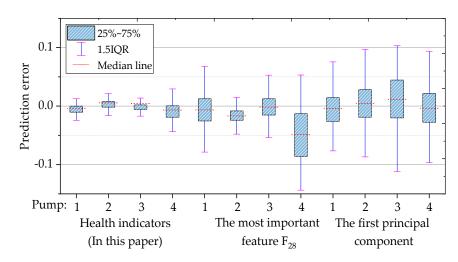
Figure 15. Box diagram of health indicator prediction deviation of four gear pumps.

According to Figure 14, it can be seen that the prediction error of the health indicator of the gear pump proposed in this paper was relatively small, and it had obvious advantages over the important feature and principal component. According to the test process, it can be seen that the equipment was in the first stage of step pressure at 0–310 h, in the second stage of step pressure at 310–733 h, in the third stage of step pressure at 733–1028 h, and in the fourth stage of step pressure at 1028–1200 h. The health states of the gear pump in the four stages of accelerating pressure were defined as health, sub-health, deterioration, and fault state.

According to the change in the step pressure loading process and running time t, the health indicators of the four gear pumps at the boundary of each health state and their mean values after removing the singularities are shown in Table 6. The numbers in boldface refer to the singularities to be removed.

Table 6. Relationship between running time and health indicators.

	Running Time	$t = 310$	$t = 733$	$t = 1028$
	Pump 1	**0.66**	0.52	0.30
	Pump 2	0.75	**0.45**	0.23
Health indicator	Pump 3	0.73	0.56	**0.48**
	Pump 4	0.75	**0.64**	0.19
	Mean value	0.74	0.54	0.24

The operating state of the gear pump was evaluated according to the average value of health indicators obtained in Table 6, and the evaluation criteria are shown in Table 7:

Table 7. Gear pump operating status division standard.

Health Indicator	Operating Status
$0.74 < HI \leq 1$	Health
$0.54 < HI \leq 0.74$	Sub-health
$0.24 < HI \leq 0.54$	Deterioration
$HI \leq 0.24$	Fault

The actual health status of the four gear pumps and their predicted health status are shown in Figure 16. In Figure 16, the health indicator is predicted and volumetric efficiency is actual. According to the figure, the health factor construction method proposed in this paper can effectively predict the health status of the gear pump, which is of great significance for timely operation and maintenance of the gear pump and early warning of the health status. It can reduce the cost of spare parts, replacement costs, and shutdown costs and bring economic benefits to enterprises.
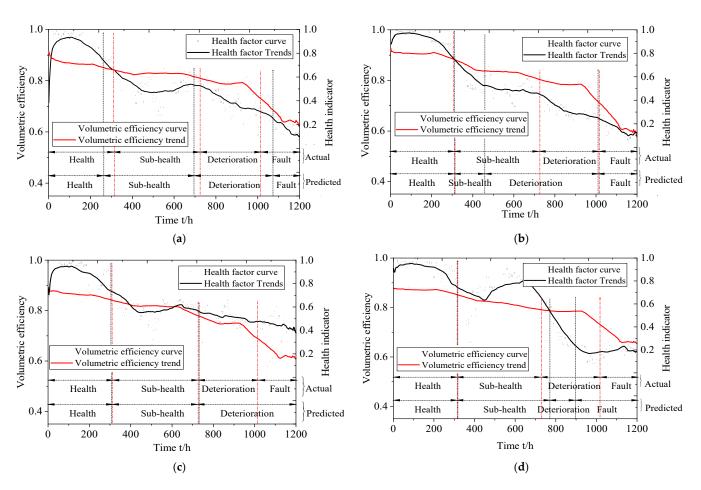
Figure 16. The actual health status and its predicted health status of gear pumps: (**a**) gear pump 1; (**b**) gear pump 2; (**c**) gear pump 3; and (**d**) gear pump 4.

6. Conclusions

In this paper, a health indicator construction and health status assessment method for gear pumps based on an LSTM–VAE is proposed. By using the vibration signal data source of the gear pump in the accelerated life test, the health indicator construction method of the gear pump based on LSTM–VAE was applied, and the one-dimensional HI curve of the whole-life operation data of the gear pump was obtained. Then, according to the volume efficiency of the gear pump, the running state of the pump was divided into four states: health, sub-health, deterioration, and fault, and the health indicator of the gear pump was applied to achieve the accurate assessment of the running state of the gear pump. Finally, the health indicator construction method of the gear pump proposed in this paper was compared with the traditional health indicator construction method, which proved the effectiveness of the proposed method. According to the theoretical research and experimental verification, the main conclusions of this paper are as follows:

(1) In terms of energy feature extraction from the wavelet packet decomposition of the gear pump, there were two frequency ranges that were highly correlated with the performance degradation characteristics, the E_{16} and E_{14} frequency bands. With the decline in the health status of the gear pump, the energy ratio of these two frequency bands showed obvious changes. In the time-domain and frequency-domain feature extraction, with the operation of the gear pump, the time-domain characteristics of the vibration signal, such as the impulse factor, peak value, root mean square value, clearance factor, and variance, showed significant changes with the change in the gear pump health status. The frequency-domain characteristics of the vibration signal, such as gravity frequency, mean square frequency, and average power, showed obvious changes with the change in the health status of the gear pump.

(2) The LSTM–VAE-based health indicator construction method of the gear pump proposed in this paper effectively constructed the one-dimensional HI curve of the whole-life operation data of the gear pump under the condition that only the health status operation data of the gear pump were needed. In addition, the proposed gear pump health indicator was superior to the traditional feature selection and PCA dimension reduction health indicator construction method in terms of trendability, robustness, and monotonicity.

(3) The health indicator of the gear pump constructed by the method proposed in this paper had an obvious correlation with the volumetric efficiency. According to the one-dimensional HI curve of the gear pump's life cycle operating data, the health status of the gear pump can be accurately assessed, which is of great significance for the intelligent operation, maintenance, and health management of gear pumps.

Since the health indicator construction and health status evaluation method proposed in this paper is based on test data, it is necessary to accumulate a large number of actual operation data of hydraulic pumps as support to apply the method to the actual hydraulic system health indicator construction and health status evaluation, train the prediction model based on the operation data, and then apply the method to the actual hydraulic system.

References

1. Tang, S.; Zhu, Y.; Yuan, S. Intelligent Fault Identification of Hydraulic Pump Using Deep Adaptive Normalized CNN and Synchrosqueezed Wavelet Transform. *Reliab. Eng. Syst. Saf.* **2022**, *224*, 108560. [CrossRef]
2. Zhang, D.; Wang, H.; Liu, J.; Wang, C.; Ge, J.; Zhu, Y.; Chen, X.; Hu, B. Flow characteristics of oblique submerged impinging jet at various impinging heights. *J. Mar. Sci. Eng.* **2022**, *10*, 399. [CrossRef]
3. Jiang, W.; Li, Z.; Li, J.; Zhu, Y.; Zhang, P. Study on a fault identification method of the hydraulic pump based on a combination of voiceprint characteristics and extreme learning machine. *Processes* **2019**, *7*, 894. [CrossRef]
4. Jiang, W.; Li, Z.; Lei, Y.; Zhang, S.; Tong, X. Deep learning based rolling bearing fault diagnosis and performance degradation degree recognition method. *J. Yanshan Univ.* **2020**, *44*, 526–536.
5. Keller, N.; Sciancalepore, A.; Vacca, A. Demonstrating a Condition Monitoring Process for Axial Piston Pumps with Damaged Valve Plates. *Int. J. Fluid Power* **2022**, *23*, 205–236. [CrossRef]
6. Sun, X.; Zhou, G.; Yu, Y.; Li, F. Overview of prognostics and health management of mechanical equipment. *Ordnance Ind. Autom.* **2016**, *35*, 30–33.
7. Xi, B.; Wang, C.; Xi, W.; Liu, Y.; Wang, H.; Yang, Y. Experimental investigation on the water hammer characteristic of stalling fluid in eccentric casing-tubing annulus. *Energy* **2022**, *253*, 124113. [CrossRef]
8. Liao, G. Data-Driven Methods of Equipment Health Assessment and Maintenance Decision-Making. Master's Thesis, Huazhong University of Science and Technology, Wuhan, China, 2016.
9. Zhang, H.; Xia, S.; Cheng, Z.; Li, X. A health assessment method of compressor based on improved Mahalanobis distance. *Electr. Meas. Instrum.* **2018**, *55*, 32–36+93.

10. Bedotti, A.; Pastori, M.; Casoli, P.; Lettini, A. Condition Monitoring Based on Thermodynamic Efficiency Method for an Axial Piston Pump. In Proceedings of the BATH/ASME 2018 Symposium on Fluid Power and Motion Control, Bath, UK, 12 September 2018.

11. Tang, S.; Zhu, Y.; Yuan, S. An adaptive deep learning model towards fault diagnosis of hydraulic piston pump using pressure signal. *Eng. Fail. Anal.* **2022**, *138*, 106300. [CrossRef]

12. Li, N.; Lei, Y.; Lin, J.; Ding, S.X. An Improved exponential model for predicting remaining useful life of rolling element bearings. *IEEE Trans. Ind. Electron.* **2015**, *62*, 7762–7773. [CrossRef]

13. Lei, Y.; Li, N.; Jing, L. A new method based on stochastic process models for machine remaining useful life prediction. *IEEE Trans. Instrum. Meas.* **2016**, *65*, 2671–2684. [CrossRef]

14. Gaperin, M.; Jurii, D.; Bokoski, P.; Viintin, J. Model-based prognostics of gear health using stochastic dynamical models. *Mech. Syst. Signal Process.* **2011**, *25*, 537–548. [CrossRef]

15. Li, H.; Wang, Y.; Bing, W.; Jian, S.; Li, Y. The application of a general mathematical morphological particle as a novel indicator for the performance degradation assessment of a bearing. *Mech. Syst. Signal Process.* **2017**, *82*, 490–502. [CrossRef]

16. Widodo, A.; Yang, B.S. Application of relevance vector machine and survival probability to machine degradation assessment. *Expert Syst. Appl.* **2011**, *38*, 2592–2599. [CrossRef]

17. Hai, Q.; Lee, J.; Jing, L.; Gang, Y. Robust performance degradation assessment methods for enhanced rolling element bearing prognostics. *Adv. Eng. Inform.* **2003**, *17*, 127–140.

18. Vasko, R.; Eljaroudi, A.; Boston, J.R.; Rudy, T.E. Hidden Markov model topology estimation to characterize the dynamic structure of repetitive lifting data. In Proceedings of the International Conference of the IEEE Engineering in Medicine & Biology Society, Chicago, IL, USA, 30 October–2 November 1997.

19. Tang, S.; Zhu, Y.; Yuan, S. Intelligent Fault Diagnosis of Hydraulic Piston Pump Based on Deep Learning and Bayesian Optimization. *ISA Trans.* **2022**, *1*, 1–16. [CrossRef]

20. Hu, B.; Wang, H.; Liu, J.; Zhu, Y.; Wang, C.; Ge, J.; Zhang, Y. A numerical study of a submerged water jet impinging on a stationary wall. *J. Mar. Sci. Eng.* **2022**, *10*, 228. [CrossRef]

21. Chao, Q.; Zhang, J.; Xu, B.; Wang, Q.; Lyu, F.; Li, K. Integrated slipper retainer mechanism to eliminate slipper wear in high-speed axial piston pumps. *Front. Mech. Eng.* **2022**, *17*, 13. [CrossRef]

22. Tang, S.; Zhu, Y.; Yuan, S. A Novel Adaptive Convolutional Neural Network for Fault Diagnosis of Hydraulic Piston Pump with Acoustic Images. *Adv. Eng. Inform.* **2022**, *52*, 101554. [CrossRef]

23. Chao, Q.; Gao, H.; Tao, J.; Wang, Y.; Zhou, J.; Liu, C. Adaptive decision-level fusion strategy for the fault diagnosis of axial piston pumps using multiple channels of vibration signals. *Sci. China Technol. Sci.* **2022**, *65*, 470–480. [CrossRef]

24. Tamilselvan, P.; Wang, P. Failure diagnosis using deep belief learning based health state classification. *Reliab. Eng. Syst. Saf.* **2013**, *115*, 124–135. [CrossRef]

25. Zhao, G.; Liu, X.; Jiang, Z.; Hu, C. Unsupervised health indicator of bearing based on deep learning. *Chin. J. Sci. Instrum.* **2018**, *39*, 7.

26. Zhu, Y.; Li, G.; Tang, S.; Wang, R.; Su, H.; Wang, C. Acoustic Signal-based Fault Detection of Hydraulic Piston Pump using a Particle Swarm Optimization Enhancement CNN. *Appl. Acoust.* **2022**, *192*, 108718. [CrossRef]

27. Tang, S.; Zhu, Y.; Yuan, S. An Improved Convolutional Neural Network with an Adaptable Learning Rate towards Multi-signal Fault Diagnosis of Hydraulic Piston Pump. *Adv. Eng. Inform.* **2021**, *50*, 101406. [CrossRef]

28. Javed, K.; Gouriveau, R.; Zerhouni, N.; Nectoux, P. Enabling health monitoring approach based on vibration data for accurate prognostics. *IEEE Trans. Ind. Electron.* **2014**, *62*, 647–656.2. [CrossRef]

29. Zhang, B.; Zhang, L.; Xu, J. Degradation feature selection for remaining useful life prediction of rolling element bearings. *Qual. Reliab. Eng. Int.* **2016**, *32*, 547–554. [CrossRef]

30. Li, Z.; Jiang, W.; Zhang, S.; Xue, D.; Zhang, S. Research on prediction method of hydraulic pump remaining useful life based on KPCA and JITL. *Appl. Sci.* **2021**, *11*, 9389. [CrossRef]

31. Liao, L. Discovering prognostic features using genetic programming in remaining useful life prediction. *IEEE Trans. Ind. Electron.* **2013**, *61*, 2464–2472. [CrossRef]

32. Li, N.; Lei, Y.; Liu, Z.; Lin, J. A particle filtering-based approach for remaining useful life predication of rolling element bearings. In Proceedings of the 2014 International Conference on Prognostics and Health Management, Cheney, WA, USA, 22–25 June 2014.